IRANIAN JOURNAL OF CATALYSIS

Synthesis, Characterization, and Antibacterial Properties of Surfactant Encapsulated Mn/Mg Co-doped Titania Nanoparticles

Sankara Rao Miditana[a*]

a)Department of Chemistry, Government Degree College, Puttur,517583, Tirupati, Andhra Pradesh, India

Received 23 July 2023; received in revised form 6 November 2023; accepted 26 November 2023 (**DOI: 10.30495/IJC.2023.1992163.2029**)

ABSTRACT

The current research work was mainly focused on the antibacterial performance of Mn/Mg co-doped TiO_2 nanoparticles in presence of Gemini surfactant (GS). Mn, Mg co-doped TiO_2 nanoparticles were synthesized by sol-gel method and calcined at 450 ^{0}C. The characterization results reveal that among all the co-doped TiO_2 and surfactant encapsulated TiO_2 nanoparticles, the MMT5-GS2 Nano catalyst exhibited the most favorable properties, featuring a small particle size, a large surface area, with respective values of 6.6 nm, 230.2 m^2/g, and a bandgap of 2.66 eV. The efficiency of the synthesized catalysts was examined by the antibacterial activity of *Escherichia coli (E. coli)* and *Klebsiella pneumonia* pathogens. Among all the catalysts, MMT5-GS2 demonstrated the best performance. The zone of inhibition of bacterial growth for *E. coli* and *Klebsiella pneumonia* was measured to be (33.1±0.12 mm) and (26.1±0.12 mm) respectively, at a concentration of 400 µg/mL. These values are significantly higher than the standard value of (chloramphenicol-16.71±0.2) at 100 µg/mL, indicating the remarkable efficacy of the MMT5-GS2 nanocatalyst**.** The co-doped nano titania particles encapsulated with surfactant have great potential as antibacterial agents.

Keywords*: Antibacterial activity, E. coli, Gemini surfactant, Sol-gel method, Visible light*

1. Introduction

Semiconducting-based photocatalysis is a widely used technology for the degradation of organic and inorganic compounds and for antibacterial activities. It involves irradiating a semiconductor with photons with energy equal to or greater than its energy gap (Eg) of the semiconductor, commonly in the UV and visible regions of the light; the electron and hole (e^-/h^+) pairs can be induced in the conduction band (CB) and valence band (VB) of the semiconductor, respectively. The e^-/h^+ pairs can, directly and indirectly, participate in the degradation of the subjected pollutant [1]. It is worth noting that among the different semiconductors that have been studied over the past few decades for their antibacterial activities, Titanium dioxide (TiO_2) stands as the most preferable one due to its non-toxicity, non-corrosive, photostability, and low cost [2-3]. TiO_2 is a widely studied and utilized material due to its unique properties, including high stability, biocompatibility, and photocatalytic activity [4]. In recent years, the development of TiO_2-based nanoparticles has attracted significant attention due to their potential applications in various fields such as energy, environment, and medicine [5]. TiO_2-based nanoparticles can be synthesized in different morphologies, such as nanoparticles, nanorods, nanotubes, and nanosheets, with varying sizes and surface modifications, allowing for the fine-tuning of their properties and applications.

The photocatalytic activity of TiO_2-based nanoparticles has been extensively studied, and it has been demonstrated that they can efficiently degrade organic pollutants and disinfect bacteria under UV or visible light irradiation [6]. In addition, TiO_2-based nanoparticles have also been explored for their antibacterial, anticancer, and drug-delivery properties. The high surface area-to-volume ratio of TiO_2-based nanomaterials, combined with their surface modification capabilities, allows for improved interaction with biological systems and enhanced performance in various applications [7].

*Corresponding author:
E-mail address: *sraom90@gmail.com* (**S. R. Miditana**)

TiO_2 is better than the rest of semiconductors for many practical applications, even though some defects limit its photocatalytic efficiency [8]. Among which, the following are important drawbacks.

a. TiO_2 has high band gap energy (3.2 eV), making it only excited with UV light, which is only 4-5% of earth's electromagnetic radiation, making it insufficient for rapid photo degradation. Artificial light sources are expensive and unstable.

b. The highest rate of electron-hole recombination occurs within nanoseconds at the TiO_2 surface, results in its low efficiency of photocatalysis.

c. Its photocatalytic activity is low in the absence of initiators (like Pt or RuO_2).

To overcome the particular limitation of TiO_2, various techniques have been employed to improve the light absorption features and lengthen the charge carrier lifetime characteristics of TiO_2, which include:

- Surface modification via organic materials.
- Semiconductor coupling.
- Band gap modification by creating oxygen vacancies.
- Doping and co-doping with non-metal and/or metals.

TiO_2-based nanoparticles can be synthesized using various chemical methods such as Sol-gel, Chemical vapor deposition, Physical vapor deposition, Chemical reduction method, Electrothermal deposition method, Hydrothermal method, and Bottom-up approaches. The choice of method depends on the desired size, shape, and composition of the nanomaterial. Among all chemical methods, the sol-gel method is a versatile and widely used chemical method for the synthesis of various types of nanomaterials, including ceramics, metal oxides, and composites. This method offers several advantages over other conventional methods, such as high control over particle size and morphology, high homogeneity and purity, low processing temperature, scalability, and versatility [9]. The sol-gel method can be easily tailored to produce nanoparticles with specific properties and structures suitable for specific applications such as catalysis, biomedicine, and electronics. Moreover, this method is a cost-effective and environmentally friendly alternative to other methods for large-scale production of nanomaterials. Therefore, the sol-gel method is a promising approach for the preparation of nanoparticles with unique properties and applications [10].

In the present work, the synthesis of Mn^{2+}, Mg^{2+} co-doped TiO_2 nanoparticles in the presence of surfactant is done using the sol-gel method. The GS is superior over conventional surfactants in terms of surface activity, and it can self-assemble at much lower concentrations. The GS is very attractive for adsorption and catalytic applications [11]. Hence, a Gemini surfactant, 1,4-Butane sultone was selected as a capping agent in the synthesis of Mn & Mg co-doped nanotitania photocatalyst. The interaction of transition metal ion dopant's (Mn^{2+}, Mg^{2+}) 3d or 4d states with the Ti 3d states results in an additional energy level below the conduction band of TiO_2, which significantly lowers the bad gap energy and electron-hole recombination compared to other metal ion dopants currently under study [12]. Manganese is most preferable among the transition metals owing to the presence of the t_2g orbital of d which is much closer to the conduction band of TiO_2 by which the absorption can be possibly shifted to the visible part of the spectrum [13]. On the other hand, Desta shumuye et al., Changneng Zhang et al., and Sofiaou et al. were investigated the effect of Magnesium, an alkaline earth metal on the crystalline structure and catalytic activity of TiO_2 and found its absorption band was shifted more towards the visible region, which led to strong photocatalytic performance [14-16]. Hence, Mn^{2+} and Mg^{2+} ions could be more effective as metal ion dopants to modify the TiO_2 for better photocatalytic performance under visible light irradiation.

The current research work was mainly focused on the antibacterial properties of *Escherichia coli* (MTCC-443) and *Klebsiella pneumonia* (MTCC- 452) of synthesized nanoparticles by measuring the zone of inhibition with respect to the standard concentration of chloramphenicol (100 µg/mL). *E. coli* and *Klebsiella pneumonia* are both types of bacteria that can cause infections in humans. The causes of these infections can vary depending on the strain of the bacteria and the site of infection. *E. coli* infections can be caused by ingesting contaminated food or water, particularly raw or undercooked meat, unpasteurized dairy products, and raw fruits and vegetables. Contact with fecal matter, either through poor hygiene practices or contaminated surfaces, can also transmit some strains of *E. coli* [17]. *Klebsiella pneumonia* is a common cause of hospital-acquired infections and can occur due to factors such as prolonged hospital stays, invasive medical procedures, and the use of certain medical devices. People with weakened immune systems, such as those with HIV/AIDS, cancer, and diabetes, are more susceptible to infections caused by both *E. coli and Klebsiella pneumonia* [18].

2. Experimental

2.1 Materials

Without additional purification, reagent-grade compounds of all types were employed in this study. Titanium tetra-n-butoxide (Ti (OBu)$_4$), Manganese nitrate [Mn (NO_3)$_2$]6H_2O, and Magnesium Nitrate [Mg (NO_3)$_2$]6H_2O purchased from E-Merck Germany were used as precursors of TiO_2, Mn and Mg respectively, for preparing Mn^{2+}/Mg^{2+} doped TiO_2 samples. 1,4-Butane sultone from Sigma Aldrich (Germany) was used for the surfactant-assisted metal doped TiO_2 catalysts.

2.2 Synthesis of Photocatalyst

Gemini surfactant-supported Mn^{2+}/Mg^{2+} doped TiO_2 samples were prepared using the sol-gel technique. During this procedure, titanium tetra-n-butoxide (10 mL) was added to ethanol (20 mL), acidified with 1.4 mL HNO_3, placed in a Pyrex glass jar (Solution-I), and stirred for 20 min. Desired wt% (0.25 wt% - 1.0 wt%) of Mn^{2+} and Mg^{2+} dopants proportional to the weight of TiO_2 into ethanol (20 mL) were taken in another beaker and added 4.5 mL of Milli-Q water to achieve efficient hydrolysis (Solution-II). Then, Solution-II was slowly added dropwise to Solution-I with continuous stirring. The colloidal solution formed after complete mixing was stirred for another 90 min and aged for 48 h to obtain a gel. The formed gel was dried (at 70 ^oC), ground, and calcined in an oven at 450 ^oC for about 5 h. After the sample has cooled, and ground sufficiently to obtain a homogeneous powder.

Following the above procedure for the preparation of different Mn and Mg co-doped catalysts by varying weight percentages of Mn & Mg (0.25 Wt% - 1.0 Wt%) as shown in **Table 1**. for the synthesis of surfactant-assisted nanoparticles, select the optimum catalyst among MMT1-MMT5. MMT5 is the best among all catalysts, so add 5 wt%, 10 wt%, and 15 wt% GS to it and synthesize surfactant encapsulated nanomaterials. For the preparation of undoped TiO_2, the above procedure is followed without the addition of Mn and Mg precursors. Details of all synthesized catalysts are shown in **Table 1**.

2.3. Experimental setup for the antibacterial activity study of photocatalyst

Antibacterial activity study of MMT5-GS2 was carried out by Agar-well diffusion method [14] against bacterial strains namely *E. coli* and *Klebsiella pneumonia* of Gram-negative pathogens. The nutrient agar (High media –India) dissolved in water was distributed in 100 mL conical flask and sterilized in an autoclave at 121 ^0C 15 lbp for 15 min. After autoclaved the media, poured into sterilized petri plates, were prepared and swabbed by using a L- shaped glass rod with 100 µL of 24 h mature broth culture of bacterial strain. The wells are made by sterile cork-borer. Wells are created in two different petri plates in the first plate undoped TiO_2, and another plate MMT5-GS2 sample solution injected (100 µg/mL, 300 µg/mL, 400 µg/mL) into the wells. The TiO_2 nanoparticles were dispersed in sterile water and it was used as a negative control, and simultaneously the standard Antibiotic Chloramphenicol (100 µg/mL) as positive control were tested against the bacterial pathogen, then the plates were incubated 24 h at 37 ^0C. The zone inhibition of every well was measured in millimetre.

3. Results and Discussion

3.1 X-ray Diffraction Study

All prepared samples (**Fig. 1a-b**), including undoped TiO_2, produced anatase peaks at 2θ values of 25.3º, 37.9º, 48.05º and 54.1º corresponding to (101), (004), (200), and (211) planes of anatase phase (JCPDS No. 21-1272). No additional peak was found at 2θ = 27.8°, indicating no rutile phase formation. Since the ionic radii of Mn^{2+} (0.78 Å) and Mg^{2+} (0.72 Å) are closer to those of Ti^{4+} (0.68 Å), it is expected that the Mn^{2+} and Mg^{2+} doped metal ions will replace the Ti^{4+} ions in the TiO_2 matrix. This is confirmed by diffraction peaks associated with Mg oxides or other compounds [19, 20]. And it is well known that since Mn^{2+} and Mg^{2+} are more electropositive, the electron cloud can remain loose in any TiO_2, favoring the formation of a less dense anatase phase [21].The average crystallite size of undoped TiO_2, MMT and MMT-GS catalysts was calculated based on the full width at half maximum (FWHM) of the characteristic high-intensity peak using the Scherrer equation, $d = k\lambda / \beta \cos\theta$ [22], where d is the average crystallite size, k is 0.9 (Scherrer's constant), λ is 1.5406 Å (X-ray wavelength), β is the FWHM and θ is the diffraction angle, listed in **Table 2**. As can be seen from the table, the average crystallite size of the catalysts ranges from 7.21-10.22 nm, 10.86-12.87 nm and 18.30 nm for MMT-GS, MMT and undoped TiO_2 nano catalysts. Substitutional doping of metal ions into the TiO_2 lattice suppresses grain growth by forming Ti-O-Mn and Ti-O-Mg, thereby reducing the crystallite size in MMT catalysts. Additional reduction in crystallite size was seen for the surfactant-prepared catalyst, which can be attributed to the Gemini surfactant's efficient capping abilities, which control the nucleation and

Table 1. Names assigned to prepared TiO_2 Nanoparticles

Entry	Weight percentages of dopants (Wt %)		Gemini Surfactant (Wt %)	Name given to the Sample
1	0.25 Mn^{2+}	0.75 Mg^{2+}	-	MMT1
2	0.75 Mn^{2+}	0.25 Mg^{2+}	-	MMT2
3	0.50 Mn^{2+}	0.50 Mg^{2+}	-	MMT3
4	1.00 Mn^{2+}	0.25 Mg^{2+}	-	MMT4
5	0.25 Mn^{2+}	1.00 Mg^{2+}	-	MMT5
6	0.25 Mn^{2+}	1.00 Mg^{2+}	5	MMT5-GS1
7	0.25 Mn^{2+}	1.00 Mg^{2+}	10	MMT5-GS2
8	0.25 Mn^{2+}	1.00 Mg^{2+}	15	MMT5-GS3
9	NIL		-	Undoped-TiO_2

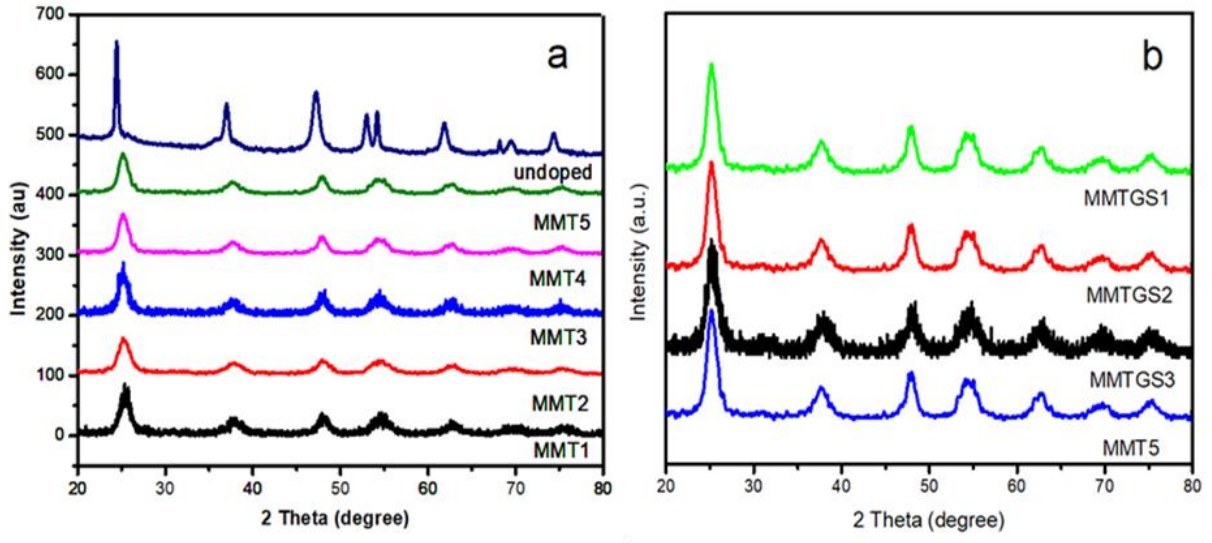

Fig. 1. (a) XRD patterns of undoped TiO_2 and Mn^{2+}/Mg^{2+} doped TiO_2 catalysts. **(b)** MMT5 and surfactant-assisted (MMT5-GS1- MMT5-GS3).

minimize the agglomeration of TiO_2 NPs during the synthesis process [23].

3.2 UV-Visible Diffuse Reflectance Spectra Study (UV–vis. DRS)

UV-vis. diffuse reflectance spectra of undoped TiO_2, MMT, and MMT-GS nanoparticles are shown in **Fig. 2a**. It can be seen that the absorption bands of MMT and MMT-GS are shifted more strongly towards higher wavelengths (redshift) compared with undoped TiO_2, which may be due to the reduced bandgap by co-doping of Mn^{2+} and Mg^{2+} into the TiO_2 matrix. The narrowing of the band gap can be attributed to the combined action of these two metal dopant ions (Mn^{2+} and Mg^{2+}) in the MMT and MMT-GS systems, which form additional energy levels below the TiO_2 conduction band, thus electron-hole recombine by trapping electrons and enhance the absorption of visible light. This can be further confirmed by the bandgap energies obtained for all synthesized catalysts using the Kubelka-Munk form. $K=(1-R)^2/2R$. In this equation, K is the reflectance transformed, and R is the reflectance (%) and the Tauc diagram method [24]. The findings validate that, in the case of co-doped semiconductors, there is an observed redshift compared to the supported doped semiconductors. Which is leading to a substantial enhancement in their photocatalytic capabilities. The corresponding band gap energy values are shown in **Table 2**. As can be seen from the table, the average bandgap values of the MMT-GS, MMT, and undoped TiO_2 photocatalysts are in the range of 2.66-2.83 eV, 2.68-2.97 eV and 3.20 eV, respectively. According to these findings, all MMT and MMT-GS catalysts are visible light active. Catalysts MMT5, MMT5-GS1, MMT5-GS2, and MMT5-GS3 have the same weight percentages of Mn and Mg; therefore, they have absorption peaks at almost the same wavelength. But in particular, MMT5-GS2 shows the lowest bandgap energy, i.e., 2.66 eV, among all MMT and GS-assisted bimetallic doped catalysts.

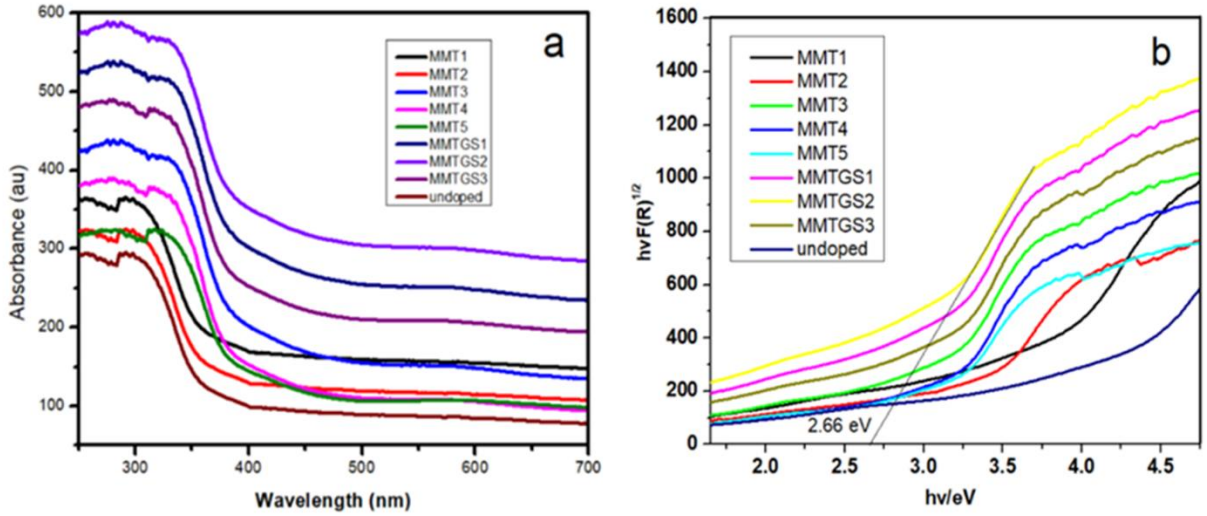

Fig. 2. (a) UV-Vis DRS and **(b)** Kubelka-Munk formalism spectra of undoped TiO_2, MMT and MMT5-GS catalysts.

Table. 2. The Results of crystallite size (XRD), Band gap (UV-Vis- DRS), and BET surface analysis

Entry	Nanomaterials	Crystallite size (nm)	Band gap energy (eV)	BET surface analysis		
				Surface area (m^2/g)	Pore volume (cm^3/g)	Pore size (nm)
1	Undoped TiO_2	18.30	3.20	64.09	0.22	10
2	MMT5	10.86	2.68	112.03	0.24	7.0
3	MMT5-GS1	10.22	2.76	140.61	0.24	7.3
4	MMT5-GS2	7.21	2.66	230.20	0.25	6.4
5	MMT5-GS3	8.33	2.83	160.14	0.22	8.3

Before proceeding to the further characterization we have conducted trial photocatalytic degradation experiments for all the synthesized catalysts using AO7 dye. From the results it was noticed that among all the bimetal doped TiO_2 catalysts, 0.25 wt% Mn^{2+}& 1.00 wt% Mg^{2+} bimetal doped TiO_2 (MMT5) exhibited better photocatalytic activity. Furthermore, MMT5 supported with 10% GS (MMT-GS2) has exhibited greater photocatalytic activity. So, we chose these two specific catalysts for additional evaluation using SEM-EDX, TEM, BET, FT-IR, and photoluminescence analysis.

3.3 SEM- Energy Dispersive X- ray Spectroscopy

The FESEM images shown in **Fig. 3a**, **b,** and **c** illustrate the surface morphology of undoped TiO_2, MMT5, and MMT5-GS2, respectively. On comparison, it can be clearly seen that the morphology of the TiO_2 has been changed from large aggregates with scratchy surfaces in undoped TiO_2 (**Fig. 3a**) to multiparticle agglomerated irregularly shaped particles with rough surfaces in MMT5 and pseudospherical less agglomerated NPs with smooth surface area and less particle size in MMT-GS2. This is clearly indicates that Mg^{2+} and Mn^{2+} bimetal ions doping and capping action with Gemini surfactant have a significant impact on the morphology of TiO_2 NPs, which controlled the grain growth and particle nucleation.

The MMT-GS2 samples were examined by EDX, and the results are shown in **Fig. 4.** Together with the Ti and O elements of TiO_2, doping elements Mn and Mg were found in the spectrum, supporting the presence of dopants in the TiO_2 matrix, and no peaks associated with GS were found in the spectrum, indicating complete elimination of GS after calcination. From the SEM results it can be inferred that agglomeration and particle size are decreased greatly in MMT-GS2 due to co-doping of Mn and Mg into TiO_2 lattice, and their presence was confirmed by EDX analysis (**Fig.4**).

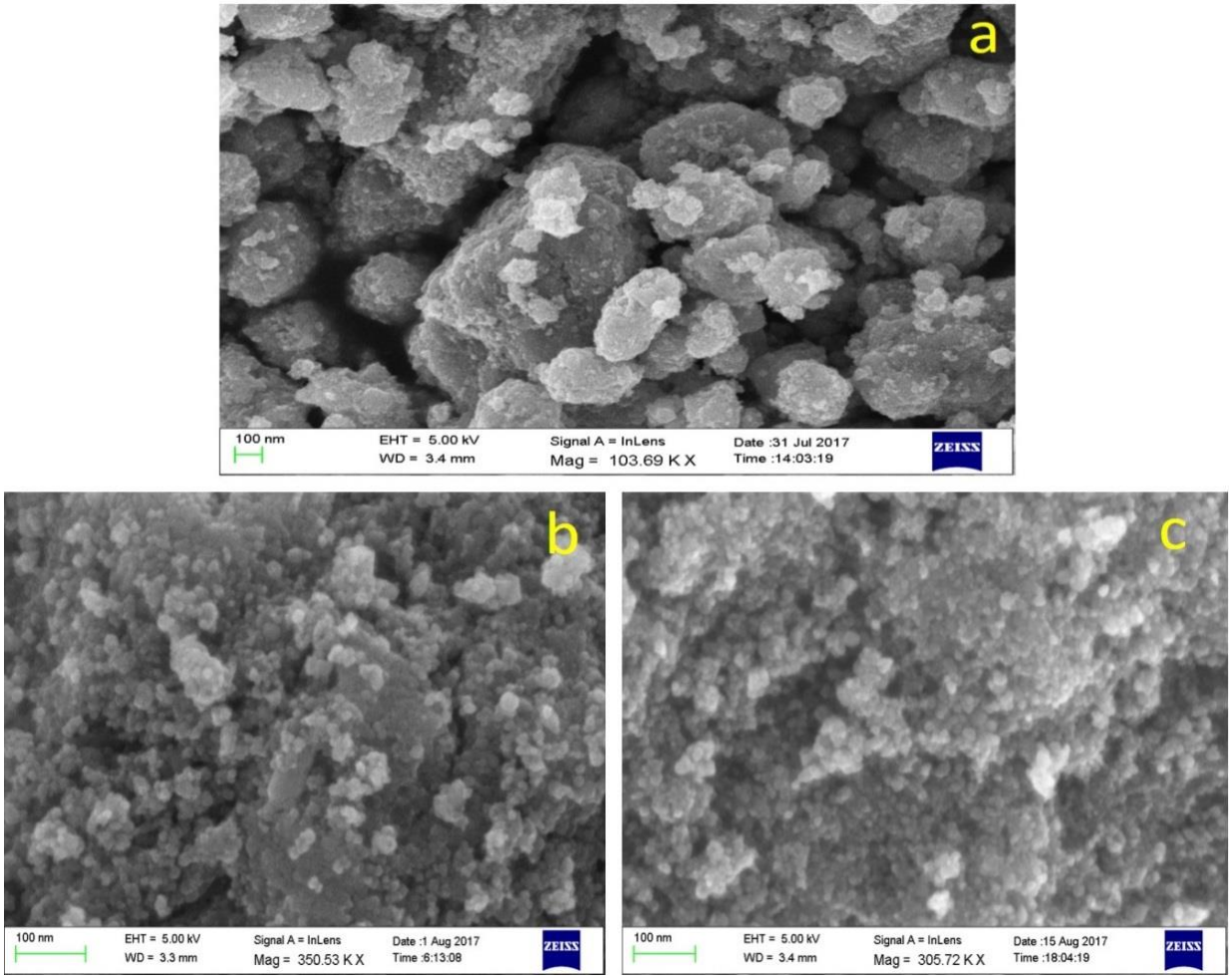

Fig. 3. SEM micrographs of **(a)** Undoped TiO_2, **(b)** MMT5 and **(c)** MMT5-GS2

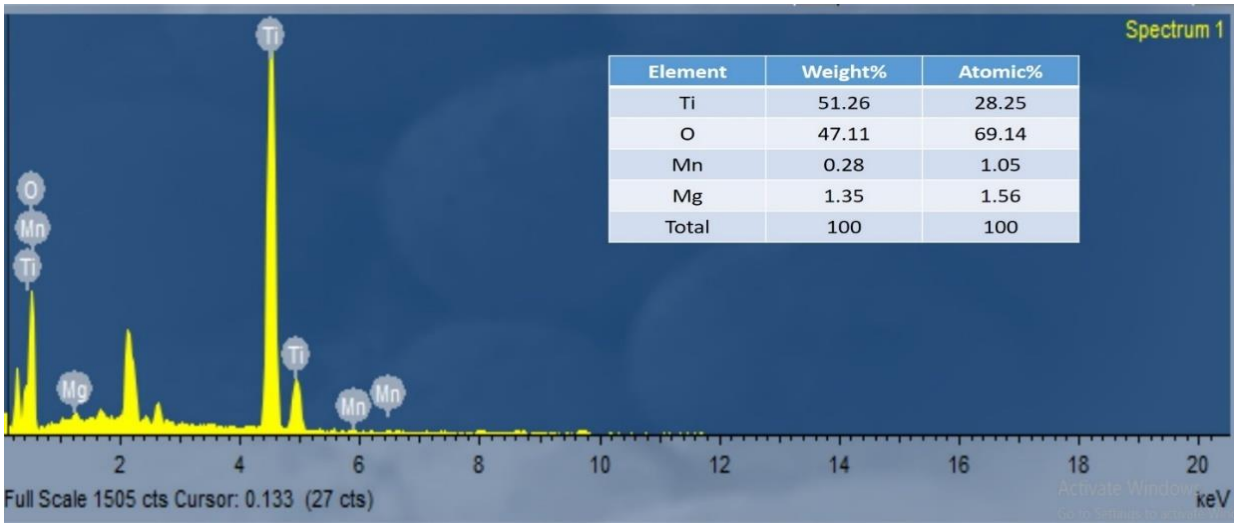

Fig. 4. EDX spectrum MMT5-GS2 after calcination with elemental composition

3.4 Transmission Electron Microscope (TEM)

In Fig. **5a** and **5b,** the TEM images of the MMT5 and MMT5-GS2 photocatalysts are given respectively. The bimetal doped TiO_2 (MMT-5) TEM image (**Fig. 5a**) displays pseudospherical shapes with multiparticle agglomeration and an average particle size of 6.6 nm. As objected to **Fig. 5a**, where the majority of the TiO_2 particles in MMT5-GS2 are well dispersed and exhibit

very little agglomeration and the particle size is in the range of 2.3-5.4 nm, with an average particle size of 3.8 nm. Thus, it clearly indicates that the Gemini surfactant was effectively inhibited the particle overgrowth and aggregation and resulted in less particle size with increased surface area, which is well correlated with BET results given in **Table 2**. The selected area electron direction (SAED) patterns shown in **Fig. 5c** confirmed the anatase phase with good crystallinity indexed by the concentric rings, which is in good agreement with XRD diffraction patterns. In addition to SAED, from the HR-TEM image of MMT5-GS2 (**Fig. 5d)** the observed lattice fringes with d-spacing of 0.352 nm correspond to (101) plane of anatase and further confirm the single crystal nature and high crystallinity of anatase TiO_2 [25].

3.5 Fourier Transform Infrared Spectroscopy (FT-IR)

The incorporation of metal ion dopants, Mn^{2+} and Mg^{2+} into TiO_2 lattice was further confirmed by FT-IR results. Fig. 6a-d displays the FT-IR spectra of the MMT5, MMT5-GS2 (both before and after calcination) and the undoped TiO_2. The peaks at 3403 cm^{-1}, 2926 cm^{-1}, 1616 cm^{-1}, 1384 cm^{-1}, 3378 cm^{-1}, 2919 cm^{-1}, 1627 cm^{-1} and 1372 cm^{-1} are corresponding to stretching vibrations of surface O-H and 3352 cm^{-1}, 2919 cm^{-1}, 1619 cm^{-1} and 1384 cm^{-1} corresponds to the and bending vibrations of adsorbed H_2O molecules [26]. The stretching vibrations of Ti-O and bending vibrations of Ti-O-Ti observed at 575 cm^{-1} and 1375 cm^{-1} in undoped TiO_2 (**Fig. 6a**) were deformed/shifted to 620 cm^{-1} and 1300 cm^{-1} in MMT5 (**Fig. 6b**) and 540 cm^{-1} and 1182 cm^{-1} in MMT5-GS2 (**Fig. 6c & 6d**) respectively, which can be attributed to the presence of dopants in TiO_2 lattice. Hence, FT-IR study confirms that Mn^{2+} and Mg^{2+} are substitutionally doped into TiO_2 lattice by replacing Ti^{4+} and formed a new network i.e. Ti-O-Mn and Ti-O-Mg which are in good agreement with the previous reports [15, 27]. The bands situated at about 2946 cm^{-1}, 1448 cm^{-1}, 1346 cm^{-1}, 1246 cm^{-1}, 1150 cm^{-1}, 1060 cm^{-1} and 997 cm^{-1} in GS were shifted to 2856 cm^{-1}, 1735 cm^{-1}, 1460 cm^{-1}, 1207 cm^{-1}, 1137 cm^{-1}, 1094 cm^{-1} and 982 cm^{-1} in MMT5-GS2 before calcinations (BC) shown in **Fig. 6c** which confirms the existence of strong electrostatic interaction between GS and catalyst surface of MMT5-GS2 before calcinations [28].

From **Fig. 6d**, the absence of these peaks confirms that there was no surfactant remained in the synthesized catalyst, MMT5-GS2 after calcination. This indicated that due to calcination at 450 °C, the surfactant is completely eliminated from the nano catalyst.

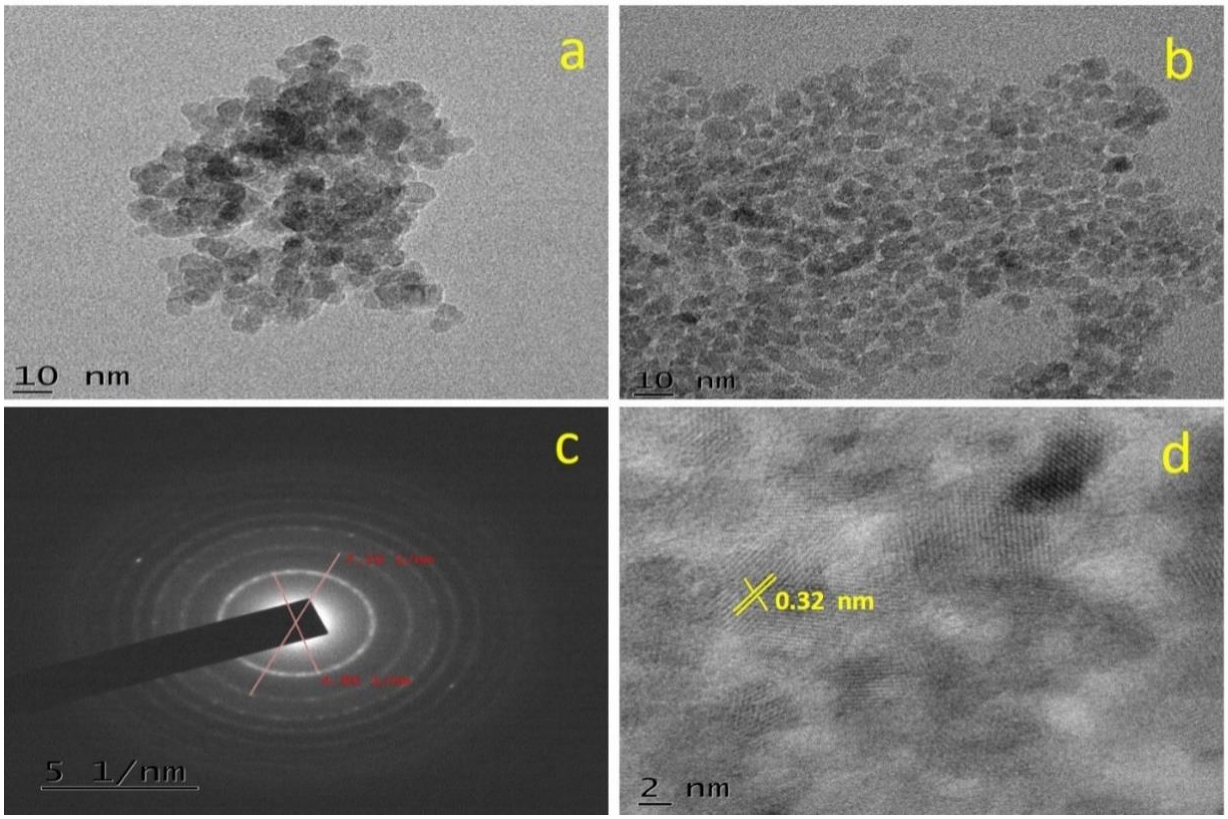

Fig. 5. TEM images of (**a**) MMT5, (**b**) MMT5-GS2, (**c**) SEAD pattern and (**d**) MMT5-GS2 using HRTEM.

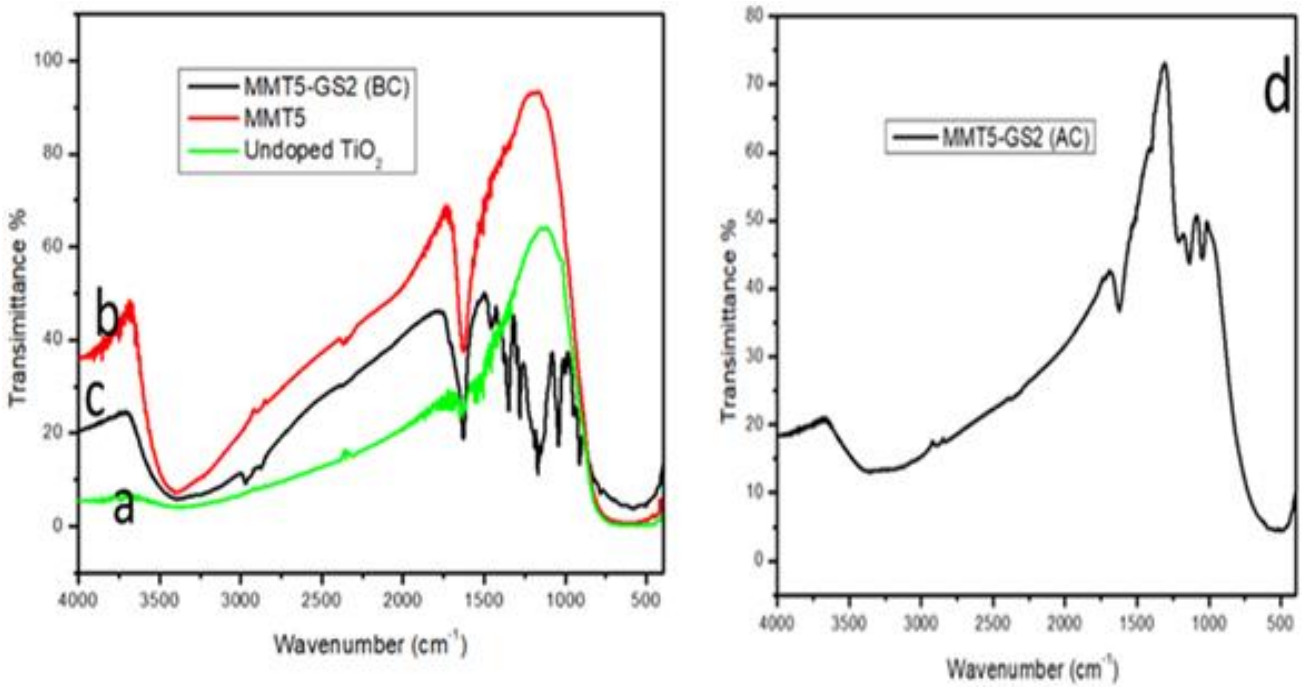

Fig. 6. (a) FT-IR spectra of undoped TiO_2, **(b)** MMT5 and (**c)** MMT5-GS2 (Before Calcination) and (**d)** FT-IR spectra of MMT5-GS2 (After Calcination)

3.6. Brunauer-Emmett-Teller (BET) surface area analysis

To examine the effect of bimetal doping and GS on the surface area and nature of the porosity of the as-produced TiO_2 nanoparticles of undoped TiO_2, MMT5, and MMT5-GS2, N_2 adsorption-desorption isotherms and their corresponding Berret- Johner- Halenda (BJH) pore size distribution plots were recorded and presented in **Fig. 7a-b**. From **Fig. 7a**, it results a type -IV isotherm with H_2 hysteresis loop, characteristic of the ordered mesoporous structure of the catalyst [29]. The average surface area, ABET (m^2/g) of all prepared catalysts was determined and tabulated in **Table 3**.

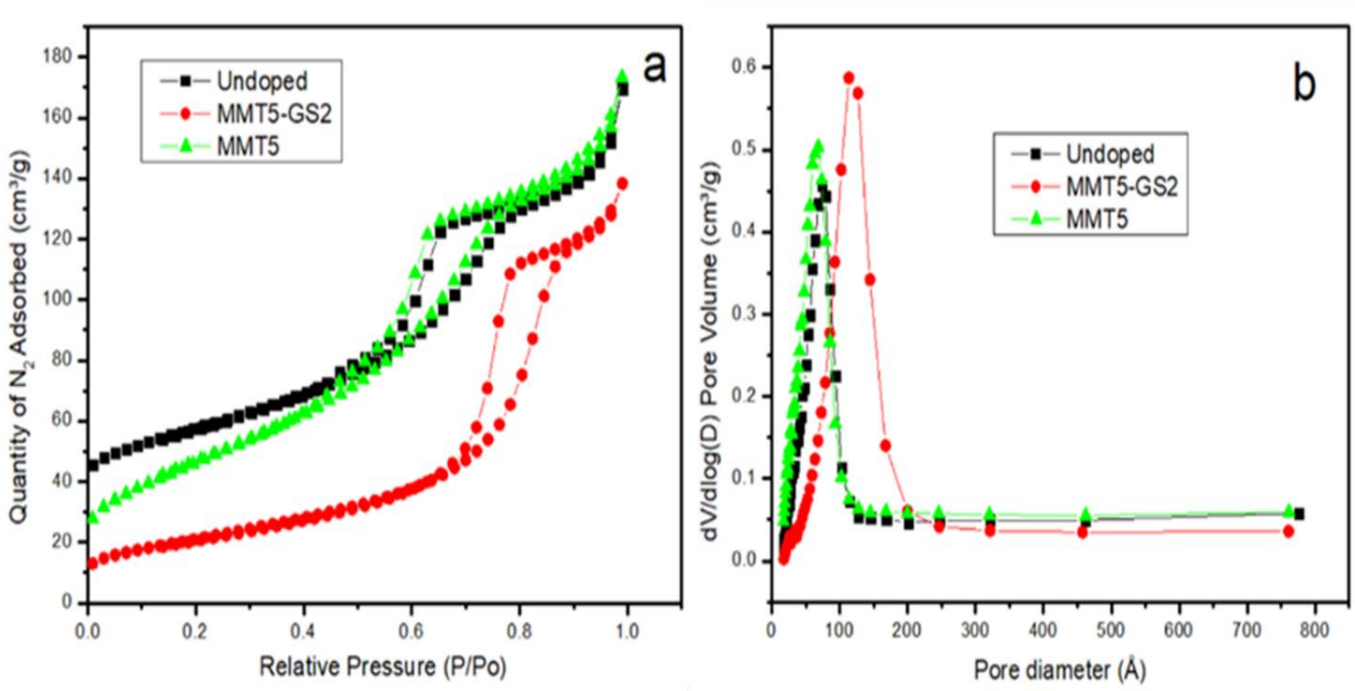

Fig. 7. (a) Isotherm of N_2 adsorption-desorption and **(b)** Distribution of pore size of undoped TiO_2, MMT5 and MMT5-GS2.

According to **Table 3**, the MMT5 has a larger surface area (112.03 m^2/g) than undoped TiO_2 (64.09 m^2/g) as a result of the dopants' suppression of crystal growth. In contrast, a catalyst made with GS surfactant (MMT5-GS2) has a greater surface area (230.20 m^2/g) than MMT5 and undoped TiO_2. It could be strong evidence for the decreased particle size of the TiO_2 resulting from the effective capping ability of the surfactant, which restricts the particle growth and nucleation during the synthesis process. Further, the MMT5-GS2 catalyst shows remarkable parameters like the band gap, surface area, and crystallite size values when compared with the Mn and Mg single-doped parameters (which are obtained from literature value) are given in **Table 3.**

3.7. Determination of efficiency of manganese and magnesium co-doped TiO_2 assisted with GS on Escherichia-coli and Klebsiella Pneumonia

The antibacterial activity of undoped and co-doped (MMT5 - GS2) TiO_2 nanoparticles was checked against different bacterial strains carried out by Agar-well diffusion method. The bacterial strains like *E. coli* (MTCC-443) and *Klebsiella pneumonia* (MTCC- 452) at different concentrations of MMT5 - GS2 nanoparticles were taken in different wells in a petri dish with a concentration ranging from 300 µg/mL, 400 µg/mL and in another well a standard chloramphenicol was taken at concentration of 100 µg/mL.

3.7.1. Determination of efficiency of Magnesium and Manganese co-doped TiO_2 assisted with GS on Escherichia Coli

The petri plates are shown in **Fig.8** (**a**) undoped and (**b**) co-doped MMT5 - GS2 catalyst. For each bacterial growth zone of inhibition diameter were determined for 3 replicates of each catalyst dosage and standard (chloramphenicol) 100 µg/mL and MMT5 - GS2 Catalyst dosage at 300 µg/mL and 400 µg/mL respectively. For each dose and standard (chloramphenicol), the mean and their standard deviation values were calculated and presented in **Table 4**. From the table the values represent the zone of inhibition of bacterial growth for *Escherichia coli* (MTCC-443) was found to be ((33.1±0.12 mm) at 400 µg/mL dose as shows 2 times better zone of inhibition of bacterial growth when compared to standard value of (chloramphenicol-16.71±0.2) at 100 µg/mL.

Table 3. Comparative table for band gap values, surface area, the crystallite size of Mn, Mg single-doped, and Mn/Mg co-doped TiO_2.

Reference	Doping Elements	Catalysts Band gap energy (eV)	Surface area (m^2/g)	Crystallite size (nm)
[30]	Mn	2.98	93	21.8
[31]	Mg	2.92	48.5	20
Present work	Mn/Mg (MMT5)	2.68	112.03	10.86
Present work	MMT5-GS2(co-doped)	2.66	230.20	7.21
Present work	undoped	3.2	64.09	18.3

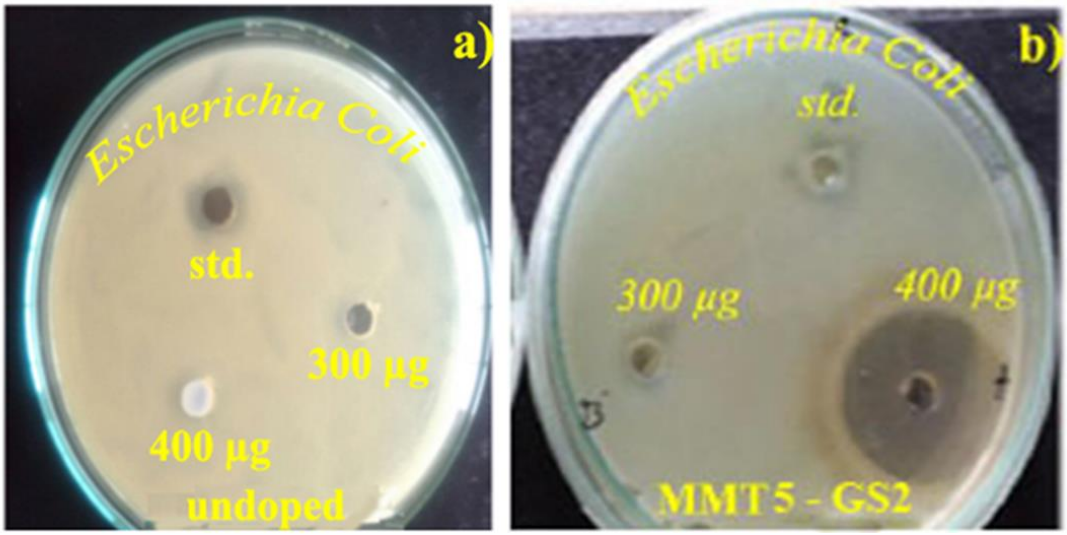

Fig. 8. Zone of inhibition of *Escherichia coli* by a) Undoped TiO_2 and b) MMT5 - GS2 Catalyst.

Table 4. Agar-well diffusion of undoped and co-doped TiO_2 nanoparticles (MMT5 - GS2) on *Escherichia coli*

Entry	Catalyst	Organism	Zone of inhibition (mm)			
			300 µg/mL	400 µg/mL	Standard 100 µg/mL	(Chloramphenicol)
1	MMT5 - GS2	*E.Coli (MTCC-443)*	11.2±0.24	33.2±0.12	16.1±0.15	
2	Undoped TiO_2	*E.Coli (MTCC-443)*	_	_	16.1±0.15	

Further, we have been calculated the T-test value for all concentrations at three replicates for each dose using SPSS software, and the calculated values are tabulated in **Table 5.** The values from the table indicated that the significant P values of each concentration is < 0.05. This is concluded that *400 µg/mL is the best concentration against the above pathogens.

3.7.2. Determination of efficiency of Manganese and Magnesium co-doped TiO_2 assisted with GS on Klebsiella pneumonia

The petri plates are shown in **Fig.9** (**a**) undoped and (**b**) co-doped MMT5 - GS2 catalyst. For each bacterial growth zone of inhibition diameter were determined for 3 replicates of each catalyst dosage and standard (chloramphenicol) 100 µg/mL and MMT5 - GS2 Catalyst dosage at 200 µg/mL, 300 µg/mL and 400 µg/mL respectively.

Table 5. Determination of mean of three replicates for a zone of inhibition of *E. coli (MTCC-443)* with MMT5 - GS2 Nano catalyst

Parameter	300 µg/mL	400 µg/mL	100 µg/mL (Standard)
Mean	11.20	33.20	16.10
SD	0.25	0.11	0.15
T-test	79.4	241.50*	170.5
P value	0.00	0.00	0.00

Mean of three replicates ± Standard deviation
*P < 0.05 was considered as significant difference

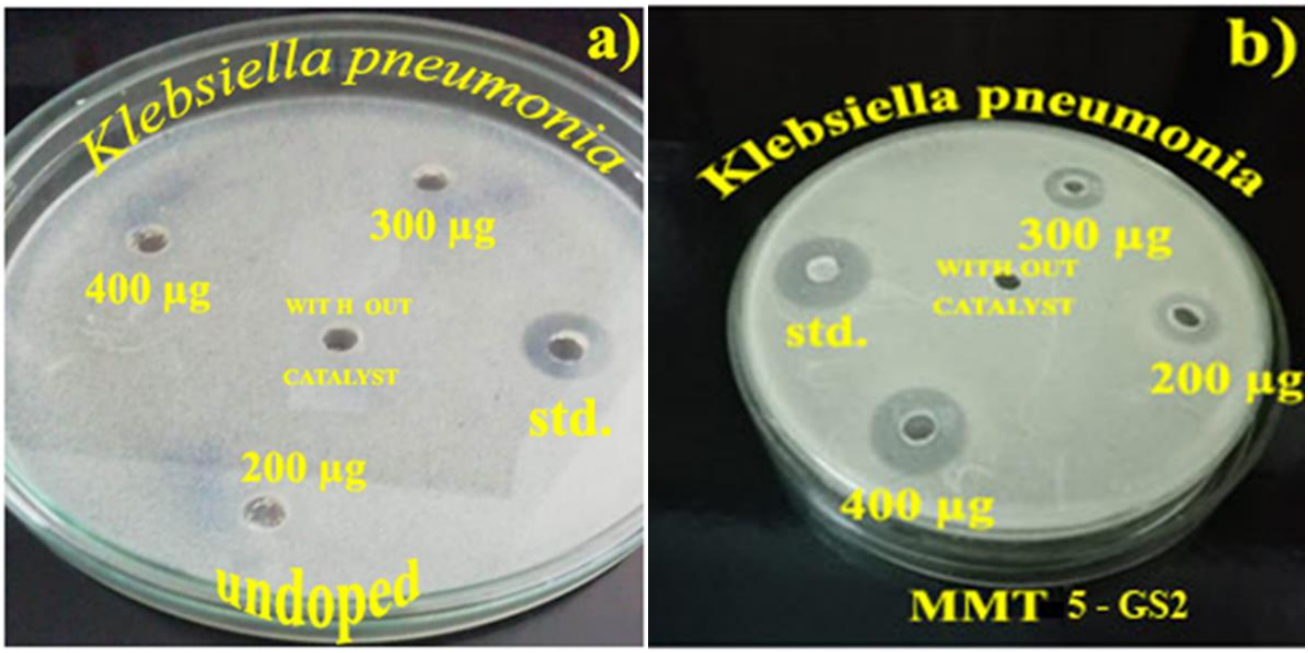

Fig. 9. Zone of inhibition of *Klebsiella pneumonia* by a) undoped TiO_2 and b) MMT5 - GS2 Catalyst

For each dose and standard (chloramphenicol), the mean and their standard deviation values were calculated and presented in **Table 6** From the table the values represent the zone of inhibition of bacterial growth for *Klebsiella pneumonia* was found to be ((26.1±0.12 mm) at 400 µg/mL dose as the better zone of inhibition of bacterial growth when compared to a standard value of (chloramphenicol 24.2±0.2) at 100 µg/mL. Further, we have been calculated the T-test value for all concentrations at three replicates for each dose using SPSS software, and the calculated values are tabulated in **Table 7.** The values from the table indicated that the significant P values of each concentration is < 0.05. This is concluded that 400 µg/mL is the best concentration against the above pathogens.

Therefore, the co-doped TiO_2 nanoparticles exhibited better antibacterial activity when compared to undoped TiO_2. This inhibition of bacterial growth may be due to an electron hole which is forms in the valance band of TiO_2 by irradiation of the catalyst with visible light. These e^-/ h^+ (+ve) acts as a strong oxidizing agent that could degrade the protein coat of the bacteria, leads to the inhibition of the growth of the organism.

Finally, based on the findings, it is revealed that the zone of inhibition of bacterial growth for *E. coli* was found to be ((33.1±0.12 mm) at 400 µg/mL dose as shows 2 times better zone of inhibition of bacterial growth when compared to standard value of (chloramphenicol-16.71±0.2) and the zone of inhibition of bacterial growth for *Klebsiella pneumonia* was found to be ((26.1±0.12 mm) at 400 µg/mL dose as better zone of inhibition of bacterial growth when compared to a standard value of (chloramphenicol 24.2±0.2). The antibacterial activity of MMT5-GS2 catalyst on *E. coli* is remarkable compared to *Klebsiella pneumonia.* And also, compare with the other dopants, Mn/ Mg co-doped nanoparticles shows the better efficiency towards antibacterial activity, which reported in the **Table 8.**

Table 6. Agar-well diffusion of undoped and co-doped TiO_2 nanoparticles (MMT5-GS2) on *Klebsiella pneumonia*

Entry	Catalyst	Organism	Zone of inhibition (mm)			
			200 µg/mL	300 µg/mL	400 µg/mL	Standard (Chloramphenicol) 100 µg/mL
1	MMT5 - GS2	*Klebsiella pneumonia* (MTCC- 452)	13.2± 0.27	18.2± 0.25	26.1± 0.21	24.2±0.15
2	Undoped TiO_2	*Klebsiella pneumonia* (MTCC-452)	_	_	_	24.2±0.2

Table 7. Determination of mean of three replicates for a zone of inhibition of *Klebsiella pneumonia* (MTCC-452) with MMT5 - GS2 nanocatalyst

Parameter	200 µg/mL	300 µg/mL	400 µg/mL	100 µg/mL (Standard)
Mean	13.20	18.02	26.10	24.21
SD	0.20	0.26	0.19	0.14
T-test	90.23	110.30	301.6*	298.50
P value	0.00	0.00	0.00	0.00

Mean of three replicates ± Standard deviation

*P < 0.05 was consider as significant difference

Table 8. Comparative table for Antibacterial performance of the other dopants with Mn/Mg co-doped TiO_2 (MMT5-GS2).

Reference	Doping Elements	Method Used	Pathogens Used	Zone of inhibition (mm)
[32]	Ag doped TiO_2	Ager diffusion method	*Escherichia Coli*	21.5± 0.33
			Pseudomonas aeruginosa	22.4± 0.68
			Klebsiella pneumoniae	21.4 ± 0.40
			Enterobacter Cloacae	24.5 ± 0.77
[33]	Cu, Ni and Cr doped TiO_2	-	*E. aerogenes*	15 ± 1.473
			B. bronchiseptica	14 ± 1.14
			S. typhimurium	19 ± 1.27
[34]	Ag, N co-doped TiO_2	Ager diffusion method	*E.Coli*	33.0
			Bacillus subtilis	22.8
Present Study	Mn, Mg co-doped TiO_2	Ager well diffusion method	*E. coli*	33.1±0.12
			Klebsiella pneumonia	26.1±0.21

3.7.3. Photocatalytic mechanism for photodegradation of bacteria

The reactive catalyst particles play a key role in the production of hydroxyl radicals ($HO^{\bullet}$) for the antibacterial activity. The photocatalytic mechanism by co-doped TiO_2 is briefly represented as follows.

The reactive catalyst particles play a key role in the production of hydroxyl radicals ($HO^{\bullet}$) for the antibacterial activity. The following steps are the prime steps for the formation of $^{\bullet}OH$. Its formation is an important step in the photocatalytic degradation of pollutants and the anti-bacterial activity of photocatalysts. When co-doped TiO_2 nano powder is irradiated with visible light, the electrons get excited to the conduction band leaving behind the holes in the valence band. The recombination of the generated electrons and holes must be prevented for effective utilization of the catalyst. Thus, generated electrons are captured by the doped dopant ions preventing their recombination [9, 35].

$$TiO_2 + h\nu \longrightarrow TiO_2 (h^+) + TiO_2 (e^-)$$

The holes react with surface bound hydroxyl groups or with water adsorbed on surface of TiO_2 to produce hydroxyl radicals and hydrogen ions.

$$TiO_2 (h^+) + H_2O \longrightarrow TiO_2 + HO^{\bullet} + H^+$$

$$TiO_2 (h^+) + HO^- \longrightarrow TiO_2 + HO^{\bullet}$$

The electrons are transferred to adsorbed oxygen producing superoxide anion.

$$`TiO_2 (e^-) + O_2 \longrightarrow TiO_2 + O_2^{\bullet -}$$

These superoxide anions further react with adsorbed water molecules producing peroxide radicals and hydroxyl ions.

$$TiO_2 (e^-) + O_2^{\bullet -} + H_2O \longrightarrow TiO_2 + HO_2^{\bullet} + HO^-$$

The peroxide radicals combine with H^+ resulting in the formation of hydroxyl radicals and hydroxyl ions. Hydrogen peroxide is formed as an intermediate product.

$$TiO_2 (e^-) + HO_2^{\bullet} + H^+ \longrightarrow TiO_2 + H_2O_2$$

$$TiO_2 (e^-) + H_2O_2 \longrightarrow TiO_2 + HO^{\bullet} + HO^-$$

Holes oxidize these hydroxyl ions to hydroxyl radicals. Thus, all the species facilitate the formation of $HO^{\bullet}$. The strong oxidants $HO^{\bullet}$ reacts with the outer part peptidoglycan of bacteria and degrade it.

$$\text{Bacteria} + HO^{\bullet} \longrightarrow \text{Products}$$

Thus, the formation of hydroxyl radicals and their role in photocatalytic activity plays an essential role in the degradation mechanism.

4. Conclusions

Successfully synthesized undoped TiO_2, $Mn^{2+,}$ and Mg^{2+} co-doped TiO_2, and anionic surfactant assisted co-doped TiO_2 nanoparticles using the sol-gel method. Various characterization techniques were employed to investigate these nanoparticle properties. FT-IR analysis confirmed the substitutional doping of Mn^{2+} and Mg^{2+} into the TiO_2 lattice, replacing Ti^{4+} and forming new networks labelled Ti-O-Mn and Ti-O-Mg. Among all the prepared nanoparticles, MMT5-GS2 stands out as superior in various parameters, featuring a crystallite size of 7.21 nm, a bandgap value of 2.66 eV, and a surface area of 230.20 m^2/g. To evaluate their efficiency, examine the antibacterial activity of these nanoparticles against gram-negative bacterial strains *E. coli* (MTCC-443) and *Klebsiella pneumonia* (MTCC-452) using the Agar-well diffusion method. Notably, the concentration of 400 µg/mL proved to be the most effective against these pathogens. In conclusion, my findings indicate that titania nanoparticles co-doped with Mn and Mg, and encapsulated with a Gemini surfactant hold significant promise as potent antibacterial agents.

Acknowledgements

Not Applicable

References

[1] A. Yousefi, A. Nezamzadeh-Ejhieh, Iran. J. Catal. 11(3) (2021) 247-259.

[2] I. Khan, K. Saeed, I. Khan, Arab. J. Chem. 12(7) (2019) 908-931.

[3] N. Baig, I. Kammakakam, W. Falath, Mater. Adv. 2 (2021) 1821-1871.

[4] X. Chen, S.S. Mao, Chem. Rev. 107(7) (2007) 2891-2959.

[5] M. Wang, L. Zhang, H. Yijja, Z. Hongwei, J.Mater.Chem.A. 9(2021)5320-5363.

[6] S. Roy, I. Hasan, B. Guo, Coord. Chem. Rev. 482(2023)215075.

[7] M.T. Noman, M.A. Ashraf, A. Ali, Environ. Sci. Pollut. Res. 26 (2019)3262-3291.

[8] A. L. Liensebiger, G. Lu, J. T. Yates, Chem. Rev. 95 (1995) 735-758.

[9] M.S. Rao,T. S. Rao, I.M. Raju, Nanosyst:. Phys. Chem. Math. 13(1) (2022)104–114.

[10] S. A. Alim, T. S. Rao, M. S. Rao, K.V. D. Lakshmi, J. Nanostructure. Chem.10 (2020) 211–226.

[11] B.S. Sekhon, Gemini (dimeric surfactants) Surfactants, Resonance. 9 (2004) 42-49.

[12] Y.Wang, R. Zhang, J. Li, S. Lin, Nanoscale. Res. Lett. 9 (2014) 46.

[13] K. V. D. Lakshmi, T. S. Rao, J. Swatipadmaja, I. M. Raju, S. A. Alim, P. Kalyani, Environ. Nanotechnol. Monit. Manage. 10 (2018)494-504.

[14] C Zhang, S. Chen, L. Y. Huang, H. Tian, Mo, L. Hu, Z. Huo, S. Dai, F. Kong, X. Pan, J. Phys. Chem. C. 115 (2011) 16418-16424.

[15] D. S. Meshesha, R. C. Matangi, T. S. Rao, B. Sreedhar, J. Asian Ceram. Soc. 5 (2017)136–143.

[16] M. V. Sofianou, M. Tassi, N. Boukos, S. Thanos, T. Vaimakis, J. Yu, C. Trapalis, Catal. Today. 230 (2014)125–130.

[17] J. B. Kaper, J. P. Nataro, H. L. Mobley, Nat. Rev. Microbiol. 2(2) (2004)123-140.

[18] T. A. Russo, C. M Marr, Clin. Microbiol. Rev. 32(3(2019) e00001-19.

[19] R. D. Shannon, Acta. Cryst. 32 (1976)751-767.

[20] N. Venkatachalam, M. Palanichamy, M. Murugesan, J. Mol. Catal. A: chem. 273(2007) 177-185.

[21] E. D. Jeong, P. Borse, J. Le, J. Ceram. Process. Res. 9(3) (2008) 250-253.

[22] H. Zabihi-Mobarakeh, A. Nezamzadeh-Ejhieh, J. Ind. Eng. Chem. 26 (2015) 315-321.

[23] J. S. Padmaja, T. S. Rao TS, K.V.D. Lakshmi, I. M. Raju, J. Environ. Chem. Eng. 6(2018)6457-6467.

[24] N. Ghobadi, Int. Nano. Lett. 3 (2013) 2.

[25] R. Jaiswal, N. Patel, D. C. Kothari, A. Miotello, Appl. Catal. B. 126(2012) 47-54.

[26] N. Venkatachalam, M. Palanichamy, B. Arabindoo, V. Murugesan, J. Mol. Catal. A: Chem. 273(2007) 177-185.

[27] N. Sharotri, D. Sharma, D. Sud, J. Mater. Res. Technol. 8 (2019)3995-4009.

[28] M. S. Rao, T. S. Rao, I. M. Raju, S. A. Alim, G. Jayasree, M. L. V. Lakshmiprasanna, Sustain. Environ. Res. 31(6) (2021)1-12.

[29] Q. R. Deng, Y. Gao, X. H. Xia, R. S. Chen, L. Wan, G. Shao, J. Phys. Conf. Ser. 152(2009) 12073.

[30] L. Maja, V. Dejan, Mater. Technol. 52(4) (2018)411- 416.

[31] A. B. Mohammad, A. Bahare, M. Nasser, Photochem. Photobiol., 87(2011) 1308–1314.

[32] T. Ali, A. Ahmed, U. Alam, I. Uddin, P. Tripathi, M. Muneer, Mater. Chem. Phys. 212(2018)325-335.

[33] S. Mumir, F. Asghar, F. Younis, S. Tabssum, RSC Adv. 12(2022) 3856.

[34] Y.Yuan, J. Ding, J. Xu, J. Deng, J. Guo, J. Nanosci. Nanotechnol. 10(8) (2010) 4868–4874.

[35] S. R. Miditana, S. R. Tirukkovalluri, I.M. Raju, A. B. Babu, A. R. Babu, J. Water. Environ. Nanotechnol. 7(2) (2022) 218-229.